Simulation-based investigation of core-shell agglomerates: influence of spatial heterogeneity in particle sizes on breakage characteristics

M. Weber[a], A. Spettl[a], M. Dosta[b,*], S. Heinrich[b], V. Schmidt[a]

[a]*Institute of Stochastics, Ulm University, Germany*
[b]*Institute of Solids Process Engineering and Particle Technology, Hamburg University of Technology, Germany*

Abstract

The stability and breakage behavior of agglomerates is of interest in many applications. Since the internal microstructure is of great influence it is very important to understand and quantify the relationship of structural properties and mechanical behavior. In this paper, we consider a flexible stochastic model to analyze the strength of spherical agglomerates consisting of spherical primary particles, arranged as core and shell. Structural properties can be varied in core and shell independently. Applying the bonded-particle model (BPM), we investigate the influence of the primary particle size distributions in core and shell on the breakage behavior under uniaxial compressive load. Moreover we perform numerical studies of the same agglomerate with different directions of force and investigate the variation in breakage behavior.

Keywords: core-shell agglomerate, discrete element method, bonded-particle model, stochastic microstructure model, compression experiment

1. Introduction

The mechanical stability of agglomerates consisting of spherical primary particles is of interest in various applications. As computational resources have become cheap and readily available, many mechanical properties can be evaluated using simulation methods. This has been done for several applications and agglomerate parameters. For instance, the effect of the agglomerate's shape on the mechanical behavior under impact load has been examined [1, 2].

The mechanical behavior under compressive load is of interest for many applications [3, 4]. Different models [5, 6, 7, 8] have been proposed for the description of forces occurring inside the agglomerate, when primary particles are in contact with each other. An overview of different models for the contact force-displacement behavior can be found in [9].

*Corresponding author, dosta@tuhh.de

Often, this is computationally studied by applying the discrete element method (DEM) extended with a bonded-particle model (BPM) [10, 11, 12], where the investigated material is represented as a set of densely packed spheres connected with ideally elastic or viscoelastic [13, 14] bonds. Opposed to experimental measurements, computational studies can give detailed information about stresses within the agglomerate. DEM simulations have been used to investigate the agglomerate breakage under impact load [2, 15, 16, 17, 18] as well as under compression [3, 19].

In [14], a flexible stochastic microstructure model for the generation of homogeneous agglomerates consisting of primary particles of two different sizes has been presented. This model has been applied to study the effect of the primary particle size distribution on the breakage behavior. But for some applications, agglomerates with a core-shell structure need to be examined [20, 21]. Current microstructure models do not cover this type of agglomerates. In this paper, we therefore extend the model presented in [14] to core-shell scenarios and evaluate the influence of spatial inhomogeneity on the breakage behavior by comparing our results to previously obtained data. Moreover, we investigate the variation of breakage behavior considering varied directions of compression. This is an important influencing factor since the investigated agglomerates are strongly anisotropic.

We investigate spherical glass agglomerates with a diameter of 8 mm which can be spatially divided into core and shell. Both, core and shell, consist of spherical primary particles of two different sizes which are bonded with hydroxypropyl methylcellulose (HPMC) binder. Main material parameters, which are used in the simulations, are listed in Table 1.

parameter	value
primary particles (glass):	
density	$2500\,\mathrm{kg/m^3}$
Young's modulus	$6 \cdot 10^{10}\,\mathrm{Pa}$
Poisson ratio	0.21
binder (HPMC):	
Young's modulus	$4 \cdot 10^{8}\,\mathrm{Pa}$
normal and tangential strength	$5 \cdot 10^{7}\,\mathrm{Pa}$

Table 1: Main material parameters of primary particles and bonds [14].

The overall packing density of primary particles is kept constant at 56 % and the mixing ratio of small and large particles is varied in core and shell. Cylindrical bonds consisting of binder material are placed between particles such that the total binder volume is 10 % of the total volume of primary particles and the ratio of the bond radius to the radius of the smallest adjacent particle is 0.4.

The rest of this paper is organized as follows. The stochastic model for generating the core-shell agglomerates is explained in Section 2, whereas the compression experiments are described in Section 3. Breakage detection and

statistical analysis of the results is done in Section 4. Section 5 concludes and gives a short outlook to possible future research.

2. Stochastic microstructure model

In the following, we describe the stochastic model used to generate the microstructure of core-shell agglomerates. Similarly to [14] the model is given by an isotropic random set. It consists of non-overlapping spherical primary particles which are fully connected by a network of cylindrical bonds.

As we want to investigate the influence of spatial heterogeneity in particle sizes on the breakage behavior, we take into account two different sizes for spherical primary particles, namely large particles with radius r_1 and small particles with radius $r_2 < r_1$. Furthermore we split the volume of the spherical agglomerate of radius r into a core with radius $r_C < r$ and a shell. For each part of the agglomerate, a mixing ratio m_C (m_S) specifies the volume fraction of large particles with respect to the overall particle volume in the core and shell, respectively. Furthermore we specify an overall packing density η.

The primary particles are generated by a packing algorithm described in Section 2.1 and connected by a network of cylindrical bonds described in Section 2.2.

2.1. Core-shell primary particle model

In this section, we extend the stochastic model introduced in [14] to generate the primary particle's structure.

Take an agglomerate radius r, a core radius $r_C < r$, a core mixing ratio m_c, a shell mixing ratio m_S, a large particle radius r_1 and a small particle radius r_2. In the first step, we transform the volumetric mixing ratios m_C and m_S into ratios of particle numbers. If large particles contribute a fraction m to the overall particle's volume, the fraction a of large particles in the overall particle count is given by

$$a = \frac{m \cdot r_2^3}{m \cdot r_2^3 + (1-m) \cdot r_1^3},$$

see [14]. We use this formula to compute the ratios of large particle numbers a_C and a_S for core and shell.

In the following steps we describe the procedure of primary particle configuration.

Step 1 First, we generate an initial configuration of possibly overlapping primary particles for the core. We draw points from the uniform distribution on the core and independently mark each point with a random radius R_C where $\mathbb{P}(R_C = r_1) = a_C$ and $\mathbb{P}(R_C = r_2) = 1 - a_C$. Each marked point corresponds to one particle. When the total volume of all particles divided by the core volume exceeds the packing density η, we discard the last particle and proceed with step 2. This results in a packing density slightly smaller than η.

Step 2 The force-biased packing algorithm [22, 23] is applied to transform the initial particle configuration into a set of non-overlapping particles inside the core.

Step 3 Similarly we generate an initial configuration of primary particles for the shell where the particles' positions are drawn from the uniform distribution on the shell and the radii are drawn from R_S with $\mathbb{P}(R_S = r_1) = a_S$ and $\mathbb{P}(R_S = r_2) = 1 - a_S$. Again, we stop generating new particles when the total volume of all particles in the shell divided by the shell volume would exceed η.

Step 4 Then we combine the already packed core particles and the (not yet packed) shell particles and apply the force-biased packing algorithm to all particles inside the agglomerate. This results in a random packing of small and large particles where the mixing ratios in core and shell can be specified separately.

An illustration of this procedure in 2D is shown in Figure 1.

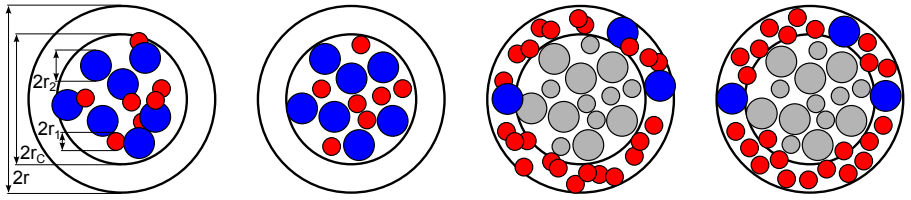

(a) Initial arrangement of core particles together with the radii r, r_C, r_1, r_2.

(b) Non-overlapping core particles after re-arrangement.

(c) Initial arrangement of shell particles, core particles in grey.

(d) Final configuration of non-overlapping particles.

Figure 1: Configuration of non-overlapping primary particles. Here, $m_C > 0.5 > m_S$, resulting in a large fraction of large particles in the core and, vice versa, in a small fraction of large particles in the shell.

2.2. Bond network model

Performing the procedure described in Section 2.1 results in a set of n non-overlapping primary particles given as sphere centers and radii $P = \{(x_i, r_i), i = 1, \dots, n\}$. In this section, we present a method for connecting the particles by cylindrical bonds such that the total volume of all bonds matches a predetermined binder volume given as a fraction b of the total volume of all primary particles. As the algorithm used in the present paper is identical to the one proposed in [14], we only give a short summary and refer to [14] for further details.

Using a threshold value l, we construct a graph $G^{(l)} = (V, E^{(l)})$ where the vertex set V represents the particles, i.e. $V = P$ and the edge set $E^{(l)}$ represents the bonds. Bonds are put between all pairs of particles with surface distance less than or equal to l. Furthermore bonds required for complete connectivity are put between particles such that the total length of all bonds remains minimal.

Given the graph $G^{(l)}$, we assign each bond $e \in E^{(l)}$ a radius $R_B(e)$ given by a fraction r_B of the radius of the smallest adjacent particle. Then we can compute the overall volume (binder volume) of the bond network. Solving an optimization problem, we get the optimal threshold value $l^\star$ such that the volume of the bond network is close to the targeted binder volume.

2.3. Model parameters

Since we want to investigate the effect of spatial heterogeneity, we vary the mixing ratios in core and shell while keeping the bond parameters, agglomerate size, packing density, small particle radius, large particle radius, and overall mixing ratio fixed.

For this we investigate the relationship between mixing ratios in core and shell and the core size. If we take a fixed core radius r_C, agglomerate radius r and fixed volumetric mixing ratios m_C and m_S in core and shell, the overall volumetric mixing ratio m is given by

$$m = \frac{r_C^3 \cdot m_C + (r^3 - r_C^3) \cdot m_S}{r^3}.$$

Solving this equation for r_C, we obtain

$$r_C = r \cdot \left(\frac{m - m_S}{m_C - m_S} \right)^{1/3}, \tag{1}$$

which only makes sense if $m_C \neq m_S$ and $\frac{m-m_S}{m_C-m_S} > 0$. For $m_C = m_S$ we can generate a particle only if $m_C = m_S = m$. In this case, the core radius can be chosen arbitrarily. For $\frac{m-m_S}{m_C-m_S} < 0$ there exists no core radius such that the desired mixing ratios can be obtained.

For a given agglomerate radius and a valid choice of parameters m, m_C, m_S, we compute the core radius r_C by Formula (1) and use these parameters along with the particle sizes and bond network parameters to generate a core-shell agglomerate using the model proposed in Sections 2.1 and 2.2.

3. Simulation of breakage behavior

For statistical analysis of breakage behavior we generate agglomerates with varied internal structures using the model introduced in Section 2. We choose the following values for the parameters of the microstructure model.

Choosing $m_S = 1 - m_C$ and $m = 0.5$ ensures that a valid core radius can be found for each core mixing ratio. In fact, except for $m_C = 0.5$,

$$\frac{m - m_S}{m_C - m_S} = \frac{1}{2}$$

is constant. So we have $r_C \approx 3.175\,\text{mm}$ for all core mixing ratios. For $m_C = m_S = m = 0.5$, we can choose any core radius, since there is no difference in

parameter	value
agglomerate:	
agglomerate radius	$r = 4\,\mathrm{mm}$
packing density	$\eta = 0.56$
primary particles:	
large particle radius	$r_1 = 0.5\,\mathrm{mm}$
small particle radius	$r_2 = 0.25\,\mathrm{mm}$
overall mixing ratio	$m = 0.5$
core mixing ratio	$m_C \in \{0, 0.1, 0.2, \ldots, 1\}$
shell mixing ratio	$m_S = 1 - m_C$
binder:	
relative binder volume	$b = 0.1$
relative bond radius	$r_B = 0.4$

Table 2: Numerical specification of model parameters.

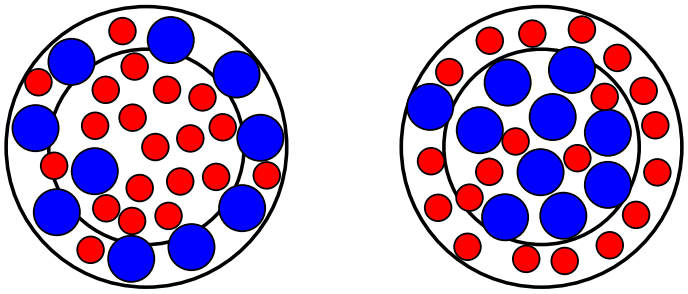

(a) Low core mixing ratio, high shell mixing ratio.

(b) High core mixing ratio, low shell mixing ratio.

Figure 2: Schematic representation of primary particles of agglomerates with different core and shell mixing ratios.

core and shell. In Figure 2, agglomerates with different core mixing ratios are visualized.

We generate 10 agglomerates for each core mixing ratio in $\{0, 0.1, 0.2, \ldots, 1\}$. Then we rotate each agglomerate according to 20 different angles distributed (almost) evenly on the sphere and for each rotated version, an uniaxial compression experiment is simulated using the DEM method.

The DEM calculations are performed with the simulation framework MUSEN [24]. The agglomerate is compressed between two walls, one of which is lowered with a constant speed. The DEM simulations are performed until the deformation of the agglomerate is 35 %. For a detailed description of the employed simulation models and parameters, see [14], Section 2.2. Simulation data such as displacement of the particles, forces applied to the particles and walls as well as breakage of bonds are recorded. Figure 3 shows the wall force for an example of a simulation run, whereas the corresponding agglomerate microstructure is

shown in Figure 4.

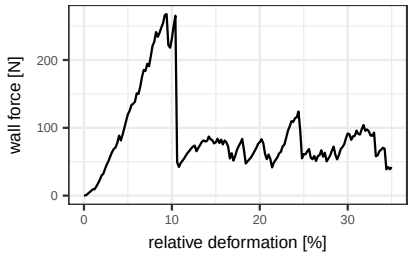

Figure 3: Wall force with respect to the deformation of a sample agglomerate with core mixing ratio 0.7.

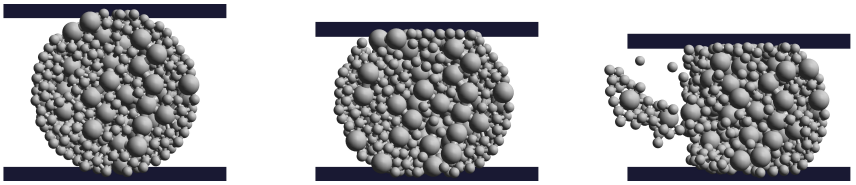

(a) 0 % deformation (b) 12.5 % deformation (c) 20.5 % deformation

Figure 4: Planar cut through agglomerate structure during DEM simulation for the same agglomerate as in Figure 3.

4. Statistical analysis

4.1. Breakage analysis

Every compression experiment gives us a force-displacement curve and the time-resolved agglomerate microstructure. Using this data we can determine the deformation at which the agglomerate breaks. As in [14] we refer to an agglomerate as broken if it consists of at least two fragments and the largest fragment comprises at most 90% of the agglomerate's volume. Debris (fragments consisting of less than 4 particles) is excluded from this analysis.

This gives us the deformation at breakage and the maximum force applied before breakage for each rotated version of each agglomerate. Furthermore, we obtain the breakage energy by integration.

The breakage characteristics for each agglomerate vary for different rotated versions. This will be discussed in Section 4.2. When comparing agglomerates to each other, it is useful to calculate the average of each characteristic over all rotated versions of one agglomerate.

Figure 5 shows the (mean) breakage characteristics for all agglomerates with different core mixing ratios. We can see that the breakage energy and deformation strongly depend on the mixing ratios in core and shell. Agglomerates

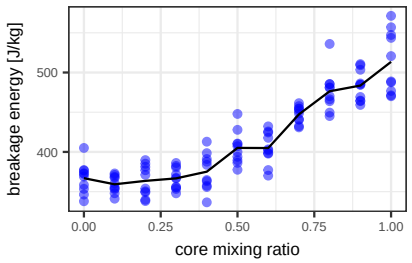

(a) Breakage energy for different core mixing ratios.

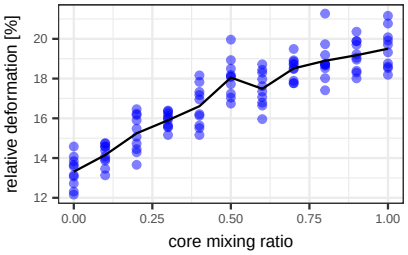

(b) Deformation at breakage for different core mixing ratios.

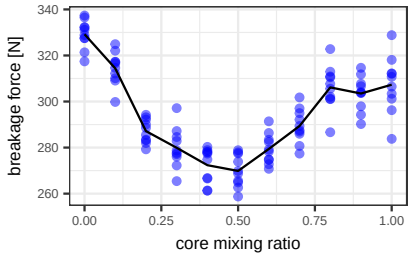

(c) Breakage force for different core mixing ratios.

Figure 5: Breakage characteristics for agglomerates with different core mixing ratios. Each point corresponds to the mean characteristic of all rotated versions of one agglomerate.

with large particles in the core and small particles in the shell (high core mixing ratio) tend to be more stable than agglomerates with small particles in the core and large particles in the shell (low core mixing ratio).

The breakage characteristics which have been obtained in [14] for homogeneous agglomerates with different overall mixing ratios are shown in Figure 6. As expected, the breakage characteristics of core-shell agglomerates with core mixing ratio 0.5 coincide with the breakage characteristics obtained in [14] for overall mixing ratio 0.5. This is due to the fact that for $m_C = 0.5$, we have $m_S = 0.5$ as well and the resulting microstructure model has no spatial inhomogeneity.

We observe that the effect of core mixing ratio on breakage energy is very similar that of (overall) mixing ratio on breakage energy obtained in [14]. This suggests that for our construction of core-shell scenarios, the microstructure of the shell does not play a significant role for the required breakage energy.

Figure 5 reveals that the breakage force for core-shell agglomerates is higher if the agglomerate has less (local) inhomogeneity in structure. This agrees with the observation in [14]. Homogeneous agglomerates have less inhomogeneity if the mixing ratio is near to 0 or 1. For core-shell agglomerates the local inhomogeneity decreases for core mixing ratios (and shell mixing ratios) near to

0 or 1, as well. Then, core and shell consist only of one sort of particles each. Local homogeneity seems to be more important than global homogeneity (i.e. core and shell are similar).

The relative deformation increases for higher core mixing ratios, i.e. for more large particles in the core. For homogeneous agglomerates, the relative deformation is highest for a mixing ratio near 0.6 and decreases for both higher and lower mixing ratios. Thus the relative deformation of core shell agglomerates seems to depend on both core and shell structure.

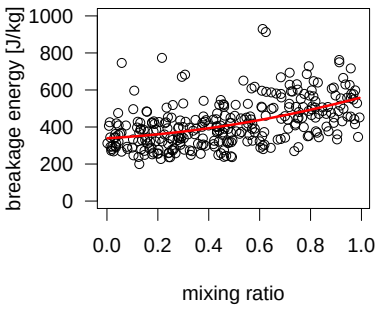

(a) Breakage energy for different mixing ratios.

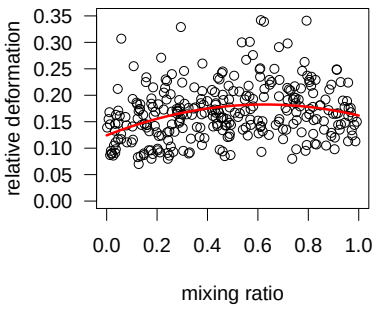

(b) Deformation at breakage for different mixing ratios.

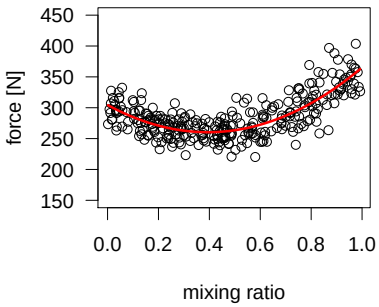

(c) Breakage force for different mixing ratios.

Figure 6: Breakage characteristics for homogeneous agglomerates with different mixing ratios. Reprinted from [14] with permission from Elsevier.

4.2. Analysis of material anisotropy

In Section 4.1, we computed a mean breakage energy for every agglomerate by performing several DEM simulations with different rotations. In this section, we investigate how different stressing directions influence the breakage energy. For the analysis of the dependence of breakage characteristics on the rotation of agglomerates, we performed 100 compression experiments for a sample agglomerate with core mixing ratio $m_C = 0.3$ which has been rotated by 100

rotation angles evenly distributed on the sphere. This results in breakage characteristics for different directions of compression. These directions are shown in Figure 7 together with the corresponding breakage energies. Since we perform uniaxial quasi-static compression experiments, the breakage characteristics do not change if we rotate the agglomerate by π in any direction. Thus, we only consider compression directions on a half sphere and copy the results for the other half by reflecting the direction through the agglomerate's center.

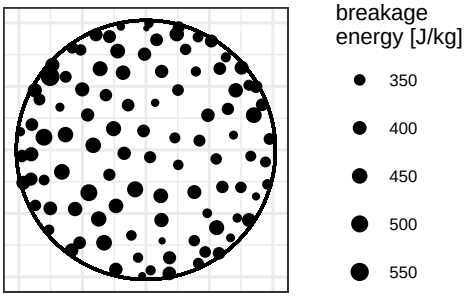

Figure 7: Distribution of the directions of compression, visualized on the half sphere. The sizes of dots correspond to the breakage energy for the corresponding rotated version of the agglomerate with core mixing ratio 0.3.

We can clearly see that the breakage energy depends on the compression direction and there seem to be clustering effects as one would expect: A small deviation in the direction of compression does result in only a small change in breakage characteristics. Thus, points corresponding to similar stressing directions have a similar size, i.e. the breakage energy is similar.

We estimate the mark correlation function for the marked point pattern $\{(S_i, L_i), i = 1, \ldots, 100\}$ given by the compression directions S_i and the breakage energies L_i as marks, applying the smallest angle between two points as distance function $d\colon (S_i, S_j) \mapsto [0, \pi]$. For the definition of the mark correlation function see [25]. The estimated mark correlation function $\theta(r)$ of the given marked point pattern $\{(S_i, L_i)\}$ can be understood as the empirical correlation between pairs of marks whose positions have distance r. This is, we compute the correlation coefficient of

$$\{(L_i, L_j) : d(S_i, S_j) = r\}$$

which is

$$\begin{aligned}\theta(r) &= \frac{\sum (L_i - \bar{L})(L_j - \bar{L})}{\sqrt{\sum (L_i - \bar{L})^2 \sum (L_j - \bar{L})^2}} \\ &= \frac{\sum L_i L_j - K\bar{L}^2}{\left|\sum L_i^2 - K\bar{L}^2\right|}\end{aligned}$$

where all sums extend over all indices $(i,j) \in \{1,\dots,100\}^2$ such that $d(S_i,S_j) = r$ and $K = |\{(L_i,L_j) : d(S_i,S_j) = r\}|$. If, in general, the marks of points with distance r were independent, we would have $\theta(r) = 0$.

Since we chose the points $\{S_i\}$ (compression directions) randomly, there exist almost surely no pairs of points with distance r. Thus, the value of $\theta(r)$ is approximated using an Epanechnikov kernel $k_{i,j}(r) = k(d(S_i - S_j) - r)$:

$$\hat{\theta}(r) = \frac{\frac{\sum k_{i,j}(r) L_i L_j}{\sum k_{i,j}(r)} - \left(\frac{\sum k_{i,j}(r) L_i}{\sum k_{i,j}(r)}\right)^2}{\left|\frac{\sum k_{i,j}(r) L_i^2}{\sum k_{i,j}(r)} - \left(\frac{\sum k_{i,j}(r) L_i}{\sum k_{i,j}(r)}\right)^2\right|},$$

where the sums extend over all pairs of indices $(i,j) \in \{1,\dots,100\}^2$.

The estimated mark correlation function (see Figure 8) confirms the visually observed clustering effects. For small differences between pairs of angles there is a significant positive correlation in the breakage energy whereas for larger differences between pairs of angles the correlation tends to 0. Thus, the breakage energy for one direction of compression can be used to predict the breakage energies for neighboring directions well but may not be a good estimate for distant directions.

For an agglomerate with a completely isotropic core and shell, we would expect the breakage energy not to depend on the direction of compression. As anisotropy decreases for larger agglomerates the differences of the relative breakage energy for different directions of force should decrease if we enlarge the agglomerate. Table 3 confirms this behavior.

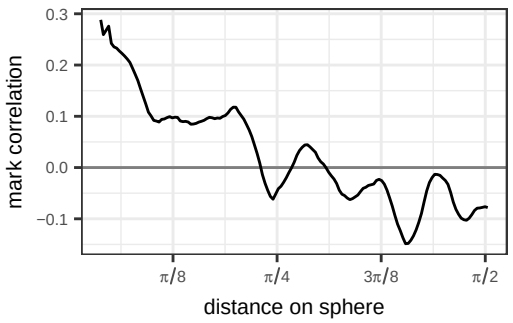

Figure 8: Estimated mark correlation function. The distance is measured in radian. For reasons of symmetry we limit the distance to $\pi/2$.

From the obtained results the conclusion can be drawn that, due to high material anisotropy, material strength strongly depends on stressing direction. Thus, in order to obtain representative information about agglomerate strength sets of simulations with varied stressing direction should be performed. For simplicity it is useful to calculate mean breakage characteristics for each agglomerate and perform the analysis on the mean values.

radius	minimum	maximum	variance
3 mm	0.253	2.054	0.327
4 mm	0.227	2.524	0.277
5 mm	0.123	2.372	0.201

Table 3: Statistics for relative breakage energy for agglomerates with different radii. Minimum and maximum are given relative to the mean breakage energy for each agglomerate.

5. Conclusion/outlook

In this paper, we extended a recently proposed model for the generation of agglomerate microstructures to core-shell scenarios while preserving the ability to control the structural properties easily. We realized a large number of comparable agglomerates with the same diameter, primary particle volume and binder volume but different primary particle radii distributions in core and shell. For simplicity we confined ourselves on special configurations of particle radii distributions. We numerically analyzed the breakage behavior for all agglomerates using the MUSEN software and applying the material properties of glass to the primary particles and HPMC to the binder. For each agglomerate we simulated several compression experiments with varied stressing directions. Finally, we analyzed the breakage behavior with respect to the primary particle mixing ratios in core and shell. The breakage energy strongly depends on the mixing ratios and increases for coarser particles in the core and finer particles in the shell. Breakage forces are higher for agglomerates with only one type of particles in each core and shell. Furthermore the breakage energy for a given agglomerate varies for different directions of force. This effect is due to inhomogeneity in small agglomerates and decreases for larger agglomerates.

These results show that breakage behavior of core-shell agglomerates can be investigated using a flexible stochastic model and DEM simulation. The primary particle size distributions in core and shell clearly affect the breakage behavior of the whole agglomerate, which differs from the behavior of the corresponding homogeneous agglomerate. Thus, even better understanding of the effects of core-shell properties to the agglomerates breakage behavior would be desirable. For this, applying the core-shell model to more complex primary particle size distributions is required. Moreover the presented methods can be extended to spatial gradients in particle size distribution and particle density which offers the possibility for the simulation of a larger range of materials.

Acknowledgments

This work was supported by the Deutsche Forschungsgemeinschaft [grant number SCHM 997/14-2] in the priority program 1679 "Dynamische Simulation vernetzter Feststoffprozesse".

References

[1] L. Liu, K. Kafui, C. Thornton, Impact breakage of spherical, cuboidal and cylindrical agglomerates, Powder Technology 199 (2) (2010) 189–196.

[2] R. Moreno, M. Ghadiri, S. Antony, Effect of the impact angle on the breakage of agglomerates: a numerical study using DEM, Powder Technology 130 (13) (2003) 132 – 137.

[3] D. Golchert, R. Moreno, M. Ghadiri, J. Litster, Effect of granule morphology on breakage behaviour during compression, Powder Technology 143–144 (2004) 84–96.

[4] A. Balakrishnan, P. Pizette, C. Martin, S. Joshi, B. Saha, Effect of particle size in aggregated and agglomerated ceramic powders, Acta Materialia 58 (3) (2010) 802–812.

[5] H. Hertz, Über die Berührung fester elastischer Körper, J. Reine u. Angew. Math. 92 (1882) 156 – 171.

[6] M. Huber, Zur Theorie der Berührung fester elastischer Körper, Ann. Phys. 12 (1904) 153–163.

[7] H. Rumpf, K. Schönert, Die Brucherscheinungen in Kugeln bei elastischen sowie plastischen Verformungen durch Druckbeanspruchung.

[8] A. Lurje, Räumliche Probleme der Elastizitätstheorie, Akademie-Verlag, Berlin, 1963.

[9] S. Antonyuk, S. Heinrich, J. Tomas, N. Deen, M. can Buijtenen, J. Kuipers, Energy absorption during compression and impact of dry elastic-plastic spherical granules, Granul. Matter 1 (2010) 15 – 47.

[10] D. Potyondy, P. Cundall, A bonded-particle model for rock, International Journal of Rock Mechanics and Mining Sciences 41 (2004) 1329–1364.

[11] M. Dosta, S. Dale, S. Antonyuk, C. Wassgren, S. Heinrich, J. Litster, Numerical and experimental analysis of influence of granule microstructure on its compression breakage, Powder Technology 299 (2016) 87–97.

[12] Z. Shen, M. Jiang, C. Thornton, DEM simulation of bonded granular material. part i: contacat model and application to cement sand, Comput. Geotech 75 (2016) 192 – 209.

[13] S. Kozhar, M. Dosta, S. Antonyuk, S. Heinrich, U. Bröckel, DEM simulation of amorphous irregular shaped micrometer-sized titania agglomerates at compression, Adv. Powder Technol. 26 (2015) 767 – 777.

[14] A. Spettl, M. Dosta, S. Antonyuk, S. Heinrich, V. Schmidt, Statistical investigation of agglomerate breakage based on combined stochastic microstructure modeling and dem simulations, Advanced Powder Technology 26 (3) (2015) 1021–1030.

[15] J. Subero, Z. Ning, M. Ghadiri, C. Thornton, Effect of interface energy on the impact strength of agglomerates, Powder Technol. 105 (1999) 66 – 73.

[16] S. Antonyuk, M. Khanal, J. Thomas, S. Heinrich, L. Mörl, Impact breakage of spherical granules: experimental study and dem simulation, Chem. Eng. Process.: Process Intensif 45 (2006) 838 – 856.

[17] M. Metzger, B. Glasser, Numerical investigation of the breakage of bonded agglomerates during impact, Powder Technol. 217 (2012) 304 – 314.

[18] Z. Tong, R. Yang, A. Yu, S. Adi, H. Chan, Numerical modelling of the breakage of loose agglomerates of fine particles, Powder Technol. 196 (2009) 213 – 221.

[19] C. Thornton, M. Ciomocos, M. Adams, Numerical simulations of diametrical compression tests on agglomerates, Powder Technol. 140 (2004) 258 – 267.

[20] K. A. Nazari, T. Hilditch, M. S. Dargusch, A. Nouri, Functionally graded porous scaffolds made of ti-based agglomerates, Journal of the Mechanical Behavior of Biomedical Materials 63 (2016) 157 – 163.

[21] S. Eckhard, M. Fries, S. Antonyuk, S. Heinrich, Dependencies between internal structure and mechanical properties of spray dried granules: Experimental study and DEM simulation, Advanced Powder Technology doi:10.1016/j.apt.2016.09.008.

[22] A. Bezrukov, M. Bargieł, D. Stoyan, Statistical analysis of simulated random packings of spheres, Particle & Particle Systems Characterization 19 (2) (2002) 111–118.

[23] J. Moscinski, M. Bargieł, Z. A. Rycerz, P. W. M. Jacobs, The force-biased algorithm for the irregular close packing of equal hard spheres, Molecular Simulation 3 (4) (1989) 201–212.

[24] M. Dosta, S. Antonyuk, S. Heinrich, Multiscale simulation of agglomerate breakage in fluidized beds, Industrial & Engineering Chemistry Research 52 (33) (2013) 11275–11281.

[25] S. N. Chiu, D. Stoyan, W. S. Kendall, J. Mecke, Stochastic Geometry and its Applications, 3rd Edition, John Wiley & Sons, Ltd, Chichester, 2013.